Hindawi
Mathematical Problems in Engineering
Volume 2018, Article ID 3043712, 12 pages
https://doi.org/10.1155/2018/3043712

*Research Article*

# Elastohydrodynamic Lubrication Characteristics of Spiral Bevel Gear Subjected to Shot Peening Treatment

**Shuai Mo**,[1,2,3,4] **Ting Zhang**,[1,2] **Guoguang Jin**,[1] **Shengping Zhu**,[1,2] **Jiabei Gong**,[1,2] **and Jingyang Bian**[1]

[1] *School of Mechanical Engineering, Tianjin Polytechnic University, Tianjin 300387, China*
[2] *The State Key Laboratory of Materials Processing and Die & Mould Technology, Huazhong University of Science and Technology, Wuhan 430074, China*
[3] *The State Key Laboratory of Mechanical Transmissions, Chongqing University, Chongqing 400044, China*
[4] *School of Mechanical Engineering & Automation, Beihang University, Beijing 100191, China*

Correspondence should be addressed to Shuai Mo; moshuai2010@163.com

Received 23 January 2018; Revised 25 March 2018; Accepted 24 April 2018; Published 10 June 2018

Academic Editor: Fabrizio Greco



High speed and heavy load put forward demanding requirements for the bending strength of spiral bevel gear. Shot peening, as a technological method, can greatly improve the bending strength of gear. During shot peening, a large number of subtle projectiles bombard the tooth surface of spiral bevel gear at an extremely high speed, which makes the latter produce plastic deformation and strengthened layer. Serving as the bombarded target, spiral bevel gear inevitably leads to the change of tooth surfaces microstructure. This paper aims at revealing the coupling law between microstructure and lubrication characteristics and establishing a reasonable model that can describe the tooth surface microstructure of shot peened spiral bevel gear. Besides, this paper brings insight into the lubrication characteristics of shot peened spiral bevel gears. Based on the elastohydrodynamic lubrication (EHL) theory, a comparative research on tooth surface lubrication characteristics has been conducted by various microscopic morphologies in this study.

## 1. Introduction

Shot peening is widely used for precision gear transmission, but lubrication and fatigue characteristics become an increasingly significant issue for shot peened gear transmission. Many scholars obtained some academic achievements by researching the lubrication and fatigue of gear transmission. Dimitrov et al. investigated the contact fatigue resistance of gear teeth by experiment and theory, and subjecting it to shot peening treatment [1]. To present a new experiment for studying contact fatigue damage of gear teeth subjected to different load patterns, Guo et al. carried out a serial sectioning procedure on shot peened 12Cr martensitic stainless steel to determine the location of fatigue crack initiation sites from pits of varying depths [2]. These results indicate that common assumptions about crack initiation from pits in shot peened steel can be misleading. Li and Anisetti proposed a contact fatigue model for spur gears operating under a high speed condition where dynamic behavior is evident [3]. A comparison between tribodynamic and quasi-static life predictions is performed to demonstrate the important role of gear tribodynamics in the fatigue damage. The impacts of the input torque, surface roughness, and lubricant temperature on the gear contact fatigue under tribodynamic condition were also investigated. Zhou et al. established a new normal stiffness model of oil film by viscous-elastic fluid between a spur gear drive equivalent and a massless spring element and proposed a tangential stiffness model according to the hypothesis of equal shear stress on laminar element surfaces [4]. It indicated that the rational parameter match is valid in mesh impact reduction and stationarity enhancement. Gallitelli et al. presented a methodology capable of producing the relation between process parameters and the state of treated part taking a complex

geometry into consideration, which include an initial state from previous manufacturing processes [5]. The proposed approach is consistent with industrial constraints in terms of computation time. The perspective is to complete the chaining process with fatigue life computations. Lv et al. studied W6Mo5Cr4V2 steel gear tooth flank by laser irradiation. Afterwards, the gear tooth flank was treated by shot peening with shot particles of different materials and peening time [6]. The experimental results showed that the hardness of gears increased and the surface roughness of gears decreased after shot peening treatment. In addition, the residual stress state in the near-surface layer of shot peened gears was changed from tensile stress to compressive stress. Terrin et al. analyzed six case hardened sun gears damaged by pitting during endurance tests [7]. All analyzed gears belonged to planetary final drives placed on a wheel hub of axles for off-highway vehicles. The aim of the analysis was to highlight the key aspects of the morphology and the evolution of pitting damage on case hardened sun gears. Pu et al. conducted a comprehensive analysis for gearing geometry, kinematics, mixed lubrication performance, and friction and interfacial flash temperature in spiral bevel and hypoid gears [8]. This study was developed based on a recently established mixed elastohydrodynamic lubrication model that was capable for handling practical cases with 3D machined roughness under severe operating conditions, considering the effect of arbitrary entrainment angle. Obtained results from sample cases showed that the developed simulation model could be used as an engineering tool for spiral bevel and hypoid gears design optimization and strength prediction. Tang et al. explored the effect of plasma molybdenizing and shot peening on fretting wear and fretting fatigue behaviors of Ti6Al4V alloy [9]. The results displayed that a beneficial residual compressive stress distribution, high surface hardness with suitable hardness gradient distribution, good apparent toughness, relatively low surface roughness, and excellent surface integrity was achieved. AlMangour and Yang made an attempt at inducing grain refinements through a shot peening process, creating severe plastic deformation at the outer surface layers, to improve the physical and mechanical properties of 17-4 stainless steel components produced by DMLS [10]. The research result highlighted the efficiency and applicability of shot peening treatment to practical cases. This contribution analytically derives a solution to the Reynolds equation to describe the longitudinal fluid pressure distribution, load capacity, and coefficient of a MHPed surface structure friction [11]. It was shown that the lateral effects in machine hammer peened surface structures significantly increased the fluid pressure. Therefore, the analytical approach presented could be used to estimate the lower bound. Simon raised an optimization methodology systematically to define the optimal tooth modifications introduced by head-cutter geometry and machine-tool settings to minimize the influence of misalignments on the elastohydrodynamic (EHD) lubrication characteristics in face-hobbed spiral bevel gears [12]. Its goal is to maximize the EHD load-carrying capacity of the oil film and to minimize power losses in the oil film when different misalignments were inherent in the gear pair. Shuai et al. developed the spiral bevel gear true tooth surface precise modeling method based on machining adjustment parameters and conducted an experiment to prove that the modeling method is right and precise. At the same time, a research in star gear transmission system was also conducted [13, 14].

Many of these researches have important effects only on elastohydrodynamic lubrication or shot peening, until now, but few literatures about elastohydrodynamic lubrication characteristics focus on shot peening. In addition, some even assume that shot peening exerts few effects on elastohydrodynamic lubrication characteristics for gear pair. Heretofore, to the best knowledge of the authors, few published studies are available on the elastohydrodynamic lubrication characteristics of shot peened spiral bevel gear. Based on the elastohydrodynamic lubrication theory, the paper making a comparative research of the tooth surface lubrication characteristics of various microscopic morphologies reveals the elastohydrodynamic lubrication characteristics of spiral bevel gears after shot peening process.

## 2. Microtopography Description of Tooth Surface by Shot Peening

Different from the roughness of tooth surface after machining, the shot peened tooth surface roughness has certain regularity. When spiral bevel gear gets into the stage of elastohydrodynamic lubrication, the oil film thickness of lubricating between the two contact tooth surfaces is in the same order of magnitude with roughness at the morphological peak of shot peened tooth surface. The materials used for shot peening mainly include ceramics, cast steel, glass, cast iron, and so on. To avoid concentrated stress points, the shape of projectile is spherical. The projectile comes in different sizes, among which the smallest diameter is 0.1 mm while the maximum reaches 2 mm. The size and material of projectile should be selected according to strengthening requirements of the sprayed workpiece, the surface roughness of workpiece, and the mechanical properties of workpiece, and so on. The strengthening effect of shot peening is related to many factors, from the material properties of workpiece and the contact distance between nozzle and workpiece to the angle of incidence. Additionally, there are shot peening speed, coverage, material type, hardness, shot peening time, projectile size, and other shot peening factors. Numerous process parameters influence the shot peening effect, and the coupling mechanisms between them are very complex.

*2.1. Construction of Multiple Projectiles' Offset Shot Peening Model.* At present, the finite element model in ABAQUS of shot peening strengthening is a multiple projectiles' offset model. As shown in Figure 1, this paper establishes the 49-pellet offset shot peening strengthening simulation model in four layers with high precision. The model assumes that the projectile is arranged in accordance with a certain law and has a bias distribution, and the target surface is vertically hit, which reduces the blind area and increases the coverage rate.

On the basis of the bias modeling method, radius of the first layer of projectiles is $R$ and the center distance is $2R$. The offset distance of the second layer relative to the first layer is $R$ in the $X$ direction, and the offset distance of the third layer

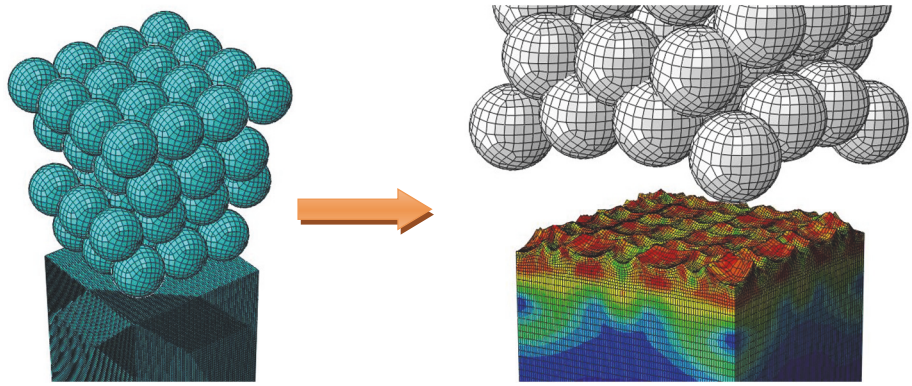

Figure 1: The finite element model of shot peening strengthening.

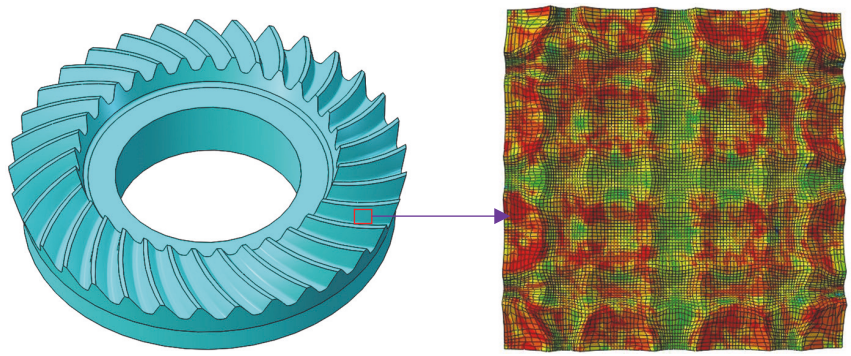

Figure 2: The surface microtopography of target tooth surface afer shot peening in ABAQUS.

relative to the first layer is $R$ in the $Y$ direction. Moreover, the offset distance of the forth layer relative to the first layer is $R$ in the $X$ and $Y$ direction, respectively. Finally, the target size is $6R \times 6R \times 12R$. There are 9 pills in the first layer, 12 pills in the second layer, 12 pills in the third layer, and 16 pills in the fourth layer.

The target material is made of high performance gear steel: 16Cr3NiWMoVNbE, and the mechanical parameters are as follows: elastic modulus: 210 GPa, density: 7800 Kg/m$^3$, Poisson's ratio: 0.3, initial yield stress: 800 MPa, hardening modulus: 1000 MPa, and coulomb friction coefficient: 0.2. Mechanical parameters of projectile are listed as follows: elastic modulus: 210 GPa, density: 7800 Kg/m$^3$, Poisson's ratio: 0.3, and initial velocity of shot peening: 50 m/s. Some constitutive model can be used for shock problem, such as Cowper-Symonds model, Johnson-Cook model, and Zerilli-Armstrong model. According to the speed of shot peening, the Cowper-Symonds constitutive model was adopted. This model is suitable for the collision of high strain rate materials. The Cowper-Symonds constitutive model has considered the strain rate in the FE model. According to the practice of engineering and references, the friction coefficient is set as 0.2.

*2.2. Construction of Surface Microtopography after Shot Peening.* Because the roughness of high precision machined tooth surface has been completely destroyed after shot peening, the roughness peak of tooth surface caused by shot peening is larger than that of grinding tooth surface. The shot peened morphology of tooth surface is the final shape. The simulation results of shot peened spiral bevel gear and the micro topography of tooth surface are shown in Figure 2. It can be seen that projectiles collide with the target surface and bounce leaving many regular craters on tooth surface. These craters overlap each other and influence each other, which completely change the microscopic appearance of spiral bevel gear tooth surface. Therefore, the orange peel pit morphology is formed on the shot peening strengthened tooth surface. In some industry situations, the shot peening strengthening coverage is even bigger, and the shot peening intensity is stronger. What is more, the pits, more irregular and smoother, have more influence on each other. The surface microstructure in this case can be used as the microstructure of shot peened gear tooth surface for studying the elastohydrodynamic lubrication characteristics of shot peening gear.

The numerical calculation of elastohydrodynamic lubrication needs to be analyzed in MATLAB, but the FEA model is built in ABAQUS, so the FEA results are necessary to be used to reconstruct the surface topography after shot peening in MATLAB. The finite element model is converted into a numerical one, extracting and exporting the deformation data of target surface in FEA to form .txt file. According to the number of surface nodes, the micro topography data of shot peened tooth surface are sorted to build a database,

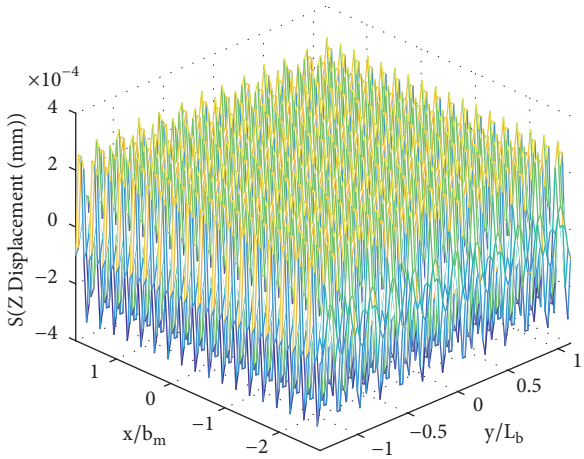


Figure 3: Reconstruction surface topography of tooth surface after shot peening in MATLAB.

which includes all data of surface topography imported to MATLAB. The three-dimensional matrix of surface topography for spiral bevel gear is established in MATLAB, and reconstruction of the surface topography is carried out. Finally, a three-dimensional nephrogram is formed, as shown in Figure 3.

## 3. Equivalent Elastohydrodynamic Lubrication Model of Spiral Bevel Gear

In fact, many factors will influence the EHL of tooth surface. In this paper, we just talk about EHL of tooth surface after shot peening treatment. Shot peening will change the microscopic geometry, and the microscopic geometry will have a big influence on EHL. The micro geometry is the most important factor for the research, so the thermal factor of EHL will be omitted. During the meshing process of spiral bevel gears, when lubricant oil film between the two contact surfaces is in the same order of magnitude with the roughness of the machined surface, the rough peak of local contact area will be contacted. At the same time, the gears are in the mixed lubrication state, and the non-Newtonian fluid characteristics are produced by strong shear acting on the lubricating oil film. Especially, under the action of extreme torque, the thickness of oil film decreases sharply and even breaks down. Therefore, the surface of metal comes in contact directly, and the tooth surface enters the dry friction state. As one of the boundary conditions of the elastohydrodynamic lubrication model, the load distribution determines the peak pressure in the contact area and the thickness of the oil film.

*3.1. Equivalent Cylindrical Gear Model of Spiral Bevel Gear.* From the engineering practice, the steady-state load distribution model is applicable when the gear rotates at a nonhigh speed. In order to establish the steady-state mixed elastohydrodynamic lubrication numerical model for long line contact in the contact area, the classical Hertz contact theory and the elastohydrodynamic lubrication theory are needed to establish the film thickness and Reynolds equation. In the end, the distribution of oil pressure and oil film thickness are figured out, and the elastohydrodynamic lubrication property of the gear pair is analyzed.

Although the tooth surface shape of spiral bevel gear is complex, it can be treated as equivalent cylindrical gear as long as operating conditions are the same, which has been proved in previous theoretical and experimental results. Furthermore, since this paper mainly explores the lubrication characteristics of spiral bevel gear shot peened tooth surface, classical elastohydrodynamic lubrication theory can be used. A two-dimensional contact elastohydrodynamic lubrication equation for long line contact is established to solve the problem of gear pair contact. According to the requirements, the entrainment velocity of contact point is regarded as $x$-axis and the direction of the contact line is regarded as $y$-axis, and $z$-axis is the normal direction of the contact area. In view of this, the model of this paper based on the equivalent cylindrical gear system is shown in Figure 4. Lubricating oil parameters are viscosity coefficient $\alpha = 2.272 \times 10^{-2}$ mm/N and dynamic viscosity $\eta_0 = 5.4{\times}10^{-8}$ Nm/mm$^2$. Gear drive parameters are shown in Table 1.

Take cylindrical gear pair as the equivalent gear pair of the spiral bevel gear; the tooth number of equivalent cylindrical gear becomes the equivalent tooth number of the spiral bevel gear. $z_v$ is the tooth number of equivalent cylindrical gear; z is the tooth number of spiral bevel gear; $\delta$ is the pitch angle of spiral bevel gear; and $d_v$ is the pitch diameter of equivalent cylindrical gear for spiral bevel gear. Based on the knowledge of mechanical principle, it can be easily obtained that $z_v = z/\cos\delta$, so $z_{v1} = z_1/\cos\delta_1$, $z_{v2} = z_2/\cos\delta_2$, $d_{v1} = mz_{v1}$, and $d_{v2} = mz_{v2}$. $N_1c$ and $N_2c$ are the radius of curvature of two contact cylinders in lubrication theory, so $N_1C = d_{v1}\sin\alpha$, and $N_2C = d_{v2}\sin\alpha$.

*3.2. Elastohydrodynamic Lubrication Control Equation*

*3.2.1. Reynolds Equation and Boundary Conditions.* In this paper, non-Newtonian fluid is chosen as lubricant, and the Reynolds equation suitable for unsteady state line contact of elastohydrodynamic lubrication is presented as follows [15]:

$$\frac{\partial}{\partial x}\left(\frac{\rho h^3}{12\eta^*}\frac{\partial p}{\partial x}\right) + \frac{\partial}{\partial y}\left(\frac{\rho h^3}{12\eta^*}\frac{\partial p}{\partial y}\right) = u_x\frac{\partial(\rho h)}{\partial x} + \frac{\partial}{\partial t}(\rho h) \tag{1}$$

In (1): $p$ and $h$ are, respectively, pressure and oil film thickness; $\eta^*$ is the equivalent viscosity of lubricating oil, $\rho$ is the density of lubricating oil; $t$ is a time variable; $\boldsymbol{\mu}_\mathbf{x}$ is the tooth surface entrainment velocity, the average value of tangential velocity of tooth surface, and $\boldsymbol{\mu}_\mathbf{x} = (\boldsymbol{\mu}_\mathbf{a} + \boldsymbol{\mu}_\mathbf{b})/\mathbf{2}$. $\mu_a$ and $\mu_b$ are the tangential velocity of tooth surface.

Equation (1) is actually a flow balance equation from the physical point of view. The first term on the left side of the equation is the pressure flow along the $X$ direction due to the pressure gradient in the fluid lubrication oil film, also known as the Poiseuille flow, while the first term on the

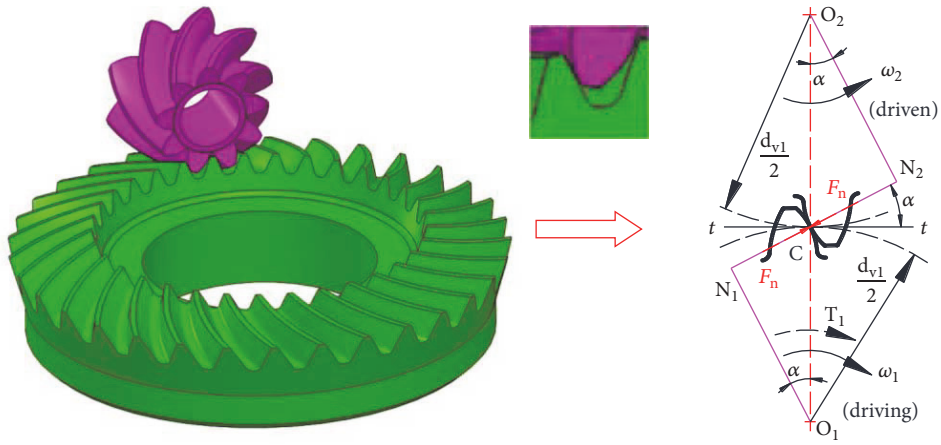


Figure 4: Spiral bevel gear meshing pair transferred to equivalent cylindrical gear meshing pair.

Table 1: Parameters of equivalent cylindrical gear pair.

| Modulus | Teeth | Pitch angle | Face wide | Rotation rate | Torque |
|---|---|---|---|---|---|
| $m$ (m) | $z_1/z_2$ | $\delta_1/\delta_2$ (°) | $B$ (m) | $n_1$ ($r$/min) | $T_p$ (Nm) |
| 0.00483 | 9/33 | 15.25/74.75 | 0.0275 | 3000 | 200 |

right indicates the shear flow due to the surface velocity, also known as the Couette flow. The second term on the right is the flow change due to the squeezing motion, which includes the change in density.

The boundary conditions of (1) are

$$p(x_{in}, t) = p(x_{out}, t) = 0,$$
$$p(x, t) \geq 0, \quad (2)$$

In (2): $x_{in}$ is the starting point coordinates of the calculation area. In this paper, $x_{in} = -4\mathbf{b}$; $\mathbf{b}$ is the half-width of Hertz contact; $x_{out}$ is the end point coordinates of the computational domain, and the value can only be determined iteratively in the numerical calculation process, instead of being set artificially.

*3.2.2. Oil Film Thickness Equation.* In the elastohydrodynamic lubrication problem, the contact deformation in the normal direction of the cylinder surface can affect the shape of the gap as shown in Figure 5. Under the action of the contact zone load, elastic deformation takes place in the normal direction of the two cylinder surfaces, which is manifested as surface indentation. Tooth surface $a$ is a rough surface, while tooth surface $b$ is a smooth one. When two elastic cylinders contact, the oil film thickness between the meshing teeth surface is

$$h(x, y) = h_0 + \Delta h + \frac{2}{\pi E'} \int\int \frac{p(x', y')}{\sqrt{(x - x')^2 + (y - y')^2}} dx' dy' - S(x, y) \quad (3)$$

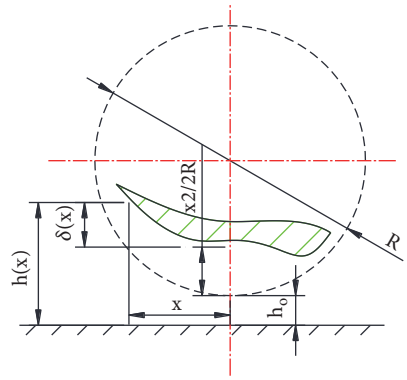


Figure 5: The gap shape for elastic deformation.

In (3): $h_0$ is a constant related to the thickness of the center of the rigid body; $\Delta h = x^2/2R$ is the variation of film thickness with the change of tooth profile in the $X$ direction; $R$ is the synthetic curvature radius of meshing point; and $E'$ represents the equivalent elastic modulus of a pair of gear teeth. $S(x, y)$ is the contact tooth surface roughness function of tooth surface $a$. This function can be a random roughness function simulated in this paper, or a function of surface topography after shot peening.

*3.2.3. Load Balance Equation.* Under the condition of no external force, the contact area of the two reverse cylinders is a line. However, when the external force is applied along the direction of the generatrix, the contact line will be extended into a contact area, and the oil film will be pressed to produce

pressure distribution in the contact area. Therefore, the load balance equation can be written as follows:

$$C_w w_n = \iint_A p(x, y)\, dx\, dy \tag{4}$$

In (4): $A$ is the total area of contact area; $C_w$ is the load coefficient; and $w_n$ is the load of each pair of meshing instantaneous target teeth. In steady-state, $C_w w_n = \mathbf{F_s}$.

*3.2.4. Rheological Model of Lubricating Oil.* Under the condition of elastohydrodynamic lubrication, the lubricant is usually subjected to high pressure and high shear stress in small contact area, where the lubricant film will withstand momentary local high pressure. Obviously, under such a high pressure, shear stress and temperature rise will lead to severe non-Newtonian characteristics of the lubricant. As for the description of rheological models, Ree-Eyrin model, J-T model, and B-W model are generally accepted.

At present, Ree-Eyrin model is often used as the rheological model of lubricant in the elastohydrodynamic lubrication model, which is applied to the unified Reynolds equation:

$$\dot{\gamma} = \frac{\tau_0}{\eta} \sinh\left(\frac{\tau}{\tau_0}\right) \tag{5}$$

In (5): $\tau_0$ is reference shear stress; $\dot{\gamma}$ is shear rate; $\eta$ is lubricating oil viscosity; and $\tau$ is oil film shear stress. Lubricating oil viscosity $\eta$ uses Roelands relation:

$$\eta = \eta_0 \exp\left\{(\ln \eta_0 + 9.67)\left[\left(1 + 5.1 \times 10^{-9} p\right)^z - 1\right]\right\} \tag{6}$$

In (6): $z$ is the viscosity index; and $\eta_0$ is environmental viscosity of lubricating oil. The equivalent viscosity $\eta^*$ satisfies the following equation:

$$\frac{1}{\eta^*} = \frac{1}{\eta}\frac{\tau_0}{\tau} \sinh\left(\frac{\tau}{\tau_0}\right) \tag{7}$$

The lubricating oil density $\rho$ uses the Dowson-Higginson formula:

$$\rho = \rho_0 \left(1 + \frac{0.6 \times 10^{-9} p}{1 + 1.7 \times 10^{-9} p}\right) \tag{8}$$

In (8): $\rho_0$ is initial density.

*3.2.5. Nondimensionalize Equations.* In general, the parameters of each basic equation need to be nondimensionalized before the operation. Dimensionless parameter is to reduce the number of variables in the dimensionless equation, so that the calculation of the equation is more convenient and easy. The paper selects frequently used and dimensionless parameter:

$$\begin{aligned} X &= \frac{x}{b_m}, \\ H &= \frac{hR_m}{b_m^2}, \\ P &= \frac{p}{p_m}, \\ \overline{\rho} &= \frac{\rho}{\rho_0}, \\ \overline{\eta} &= \frac{\eta}{\eta_0}, \\ k_n &= \frac{L_b}{b_m}, \\ \overline{t} &= \frac{u_m t}{b_m} \end{aligned} \tag{9}$$

In (9): $\rho_0$ is environmental density of the lubricating oil; $\eta_0$ is environmental viscosity of the lubricating oil; $R_m$ is the synthetic curvature radius of pitch point, and $\mu_m$ is the entrainment velocity of pitch point. The expressions of Hertz contact area half-width and peak pressure of pitch point under load are as follows:

$$\begin{aligned} b_m &= \sqrt{\frac{4w_m R_m}{\pi E' L_b}}, \\ p_m &= \frac{w_m}{\pi b_m L_b} \end{aligned} \tag{10}$$

Add formula (9) and formula (10) to (1) and to (4), and the dimensionless elastohydrodynamic lubrication control equation can be obtained.

$R$ is the synthetic curvature radius of two contact surfaces, and the curvature radius of surface 1 and surface 2 is $R_1$ and $R_2$. The relation between them is

$$\frac{1}{R} = \frac{1}{R_1} + \frac{1}{R_2} \tag{11}$$

$E'$ is a synthetic elastic modulus of two surface solid materials, and $E_1$ and $E_2$ are the elastic modulus of solid 1 and solid 2. $\sigma_1$ and $\sigma_2$ are Poisson's ratio. The relation between them is as follows:

$$\frac{1}{E'} = 0.5\left(\frac{1 - \sigma_1^2}{E_1} + \frac{1 - \sigma_2^2}{E_2}\right) \tag{12}$$

For the steady-state, the gear pair is equivalent to a pair of reverse disc rollers with different curvature radius at each meshing position, and the load of each roller is different. With steady load distribution as the boundary conditions of elastohydrodynamic lubrication equation, if the numerical calculation of the lubrication state of the meshing gear at the pitch circle is carried out, the changing rule of pressure

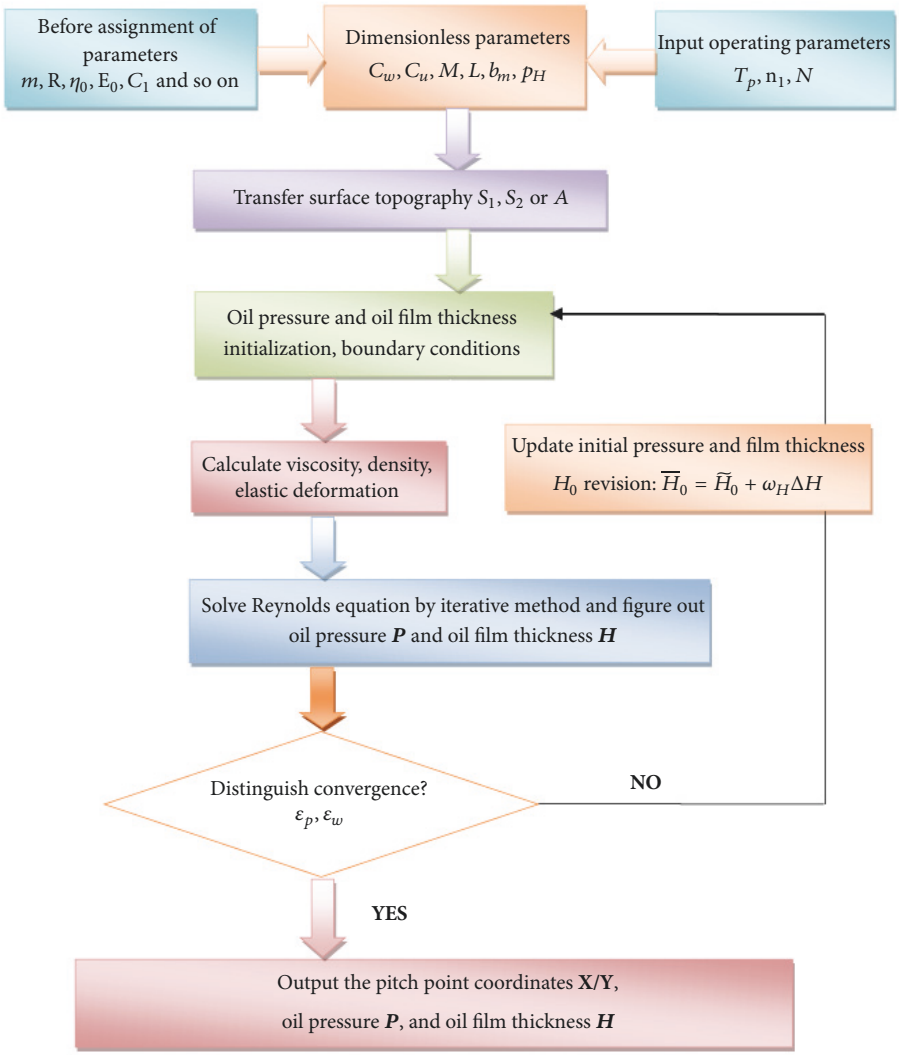


Figure 6: Flowchart of elastohydrodynamic lubrication analysis.

distribution and oil film thickness at this instant will be obtained. The lubrication state of the whole area is expressed by the state of the elastic fluid lubrication of the meshing gear at this position, and then the elastohydrodynamic lubrication characteristics of the gear can be calculated.

*3.2.6. Calculation Flow Chart.* The Reynolds equation is solved by iteration method, the Gauss-Seidel relaxation method is used. Each cycle is determined by two convergence criteria $\varepsilon_p$ and $\varepsilon_w$ to determine whether to continue the cycle or to jump out of the cycle to output pressure and film thickness, such as formula (13). Figure 6 provides a flowchart for the calculation of two-dimensional finite line contact steady-state hybrid elastohydrodynamic lubrication.

$$\begin{aligned} \varepsilon_p \frac{\sum\sum \left| p_{i,j}^{k+1} - p_{i,j}^{k} \right|}{\sum\sum p_{i,j}^{k+1}} &\le 1e-4, \\ \varepsilon_w \frac{\left| C_w \pi k_n - h_x^k h_y^k \sum\sum p_{i,j}^{k} \right|}{\sum\sum p_{i,j}^{k}} &\le 1e-4 \end{aligned} \tag{13}$$

## 4. Lubrication Characteristics: Oil Pressure Distribution and Oil Film Thickness

Elastohydrodynamic lubrication analysis of the multiple projectiles' offset shot peening model can well observe the impact of a single crater during lubrication, and the effect study of shot peening on elastohydrodynamic lubrication after the whole micro surface is reshaped. As the pits formed by shot peening strengthening with 9-pellet model and 25-pellet model have no interaction, it is more practical to study the elastohydrodynamic lubrication after shot peening strengthening with the 49-pellet model. With the increase of shot peening coverage, craters will affect each other, and the bulge around a single crater may be hit by a large number of pellets. Thus, the impact of bulge will be weakened.

Figures 7 and 8 show the three-dimensional distribution profile of elastohydrodynamic lubrication oil pressure and oil film thickness after shot peening in meshing tooth surface of spiral bevel gear. Figure 7 is the oil pressure distribution in meshing tooth surface for spiral bevel gear during elastohydrodynamic lubrication. $X$ direction is $b_m$; $b_m$ stands for

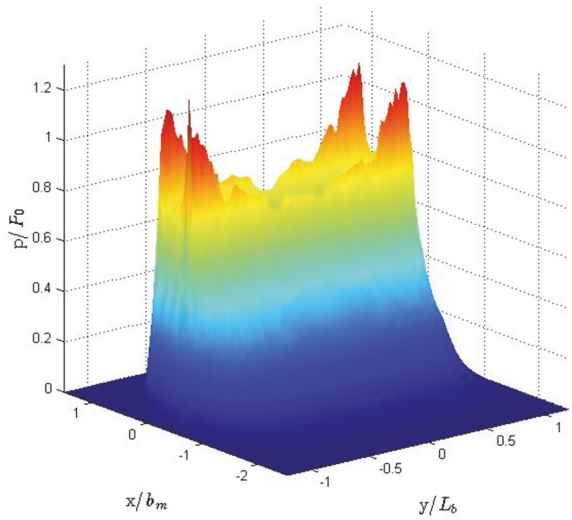


Figure 7: Oil pressure distribution in meshing tooth surface of spiral bevel gear.

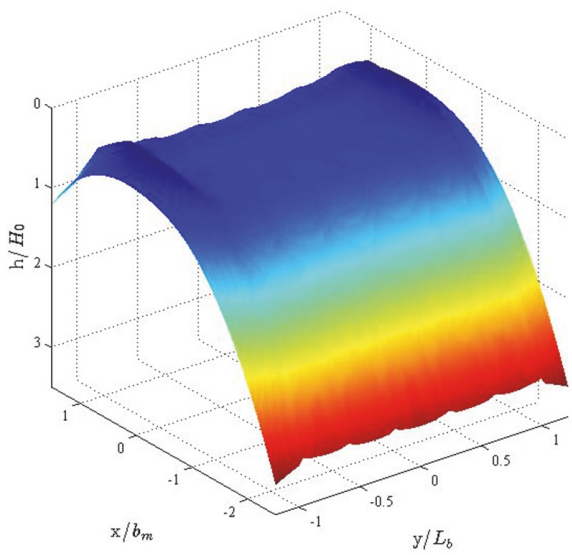


Figure 8: Oil film thickness distribution in meshing tooth surface of spiral bevel gear.

half-width of Hertz contact zone; $Y$ direction is $L_b$; $L_b$ stands for the length of contact line.

According to the rule of Figures 7 and 8, in addition to three basic rules of the elastic fluid lubrication, oil film thickness, and oil pressure distribution, the orange peel pits are connected with each other, and the effect of pits on the elastohydrodynamic lubrication characteristics is more obvious. On the other hand, along the direction of meshing line, the influence of pits on the lubrication characteristics is smaller than that in the $x$ direction, which is the entrainment velocity direction. This is because the oil pressure and oil film thickness are greatly affected by the load and the entrainment velocity. The transverse flow of the lubricant, omitted in principle, in the direction of meshing line is very small. In the direction of entrainment velocity, the bulge formed around the orange peel pit seriously hinders the flow of oil. Pressure increases here, and local pressure value even exceeds the second peak value $1.2P_0$ and reaches the highest value $1.3P_0$, while the oil film thickness decreases. Furthermore, it is very easy to produce oil film rupture, resulting in rough peak contact, which will increase tooth surface wear.

Figure 9 shows the oil pressure and oil film thickness distribution in the $y = 0, x = 0$ section. The purple dotted line stands for oil film thickness and the red solid line stands for oil pressure. Meanwhile, combined with Figures 9(a) and 9(b), these two sections are passed through the center of pit. $X$ direction is $b_m$; $b_m$ stands for half-width of Hertz contact zone; $Y$ direction is $L_b$; $L_b$ stands for the length of contact line.

As shown in Figure 9(a), along the $x$ direction, the pressure is concentrated on the Hertz contact area. There is a marked decrease of oil pressure in the contact area, where peak pressure value falls from $0.8P_0$ on both sides to $0.6P_0$ in the pit, and the pressure drops about 25%. The oil film thickness increases from $0.55H_0$ to $0.6H_0$, and the film thickness raises about 10%.

However, as shown in Figure 9(b), along the $y$ direction, peak oil pressure value descends from $0.7P_0$ on both sides to $0.65P_0$ in the pit, and the pressure falls about 7%. The oil film thickness increased from $0.5H_0$ to $0.58H_0$, and the oil film thickness grows about 16%.

It is proved again that the pit has a greater influence on the pressure distribution in the direction of entrainment velocity, and the influence on the oil film thickness is smaller than that of the pressure. But, in general, due to the local oil pressure around the orange peel pit, a large amount of lubricating oil flows to the orange peel pit. Therefore, with much lubricating oil accumulated in the orange peel pit, the oil film thickness is increased, which is favorable for lubrication.

The roughness function is used to simulate tooth surface roughness of spiral bevel gear. The distribution function of tooth surface roughness is $S = R_s \cos(2\pi x/w_x) \cos(2\pi y/w_y)$. Figure 10 is the graph for effects on oil pressures distribution with different roughness level surfaces. S-P is short for shot-penning; Figure 10(a) is $y = 0$ section; and Figure 10(b) is $x = 0$ section. Figure 11 is the graph for effects on oil film thickness distribution with different rough level surfaces. S-P is short for shot-penning; Figure 11(a) is $y = 0$ section; and Figure 11(b) is $x = 0$ section. $X$ direction is $b_m$; $b_m$ stands for half-width of Hertz contact zone; $Y$ direction is $L_b$; $L_b$ stands for the length of contact line.

Intuitively, asperity has great effects on both oil pressure and oil film thickness, but the effect on oil pressure is relatively greater than that on oil film thickness. The asperity of shot peened microsurface becomes less, and those ridges that prevent the lubrication also connect into one piece. Therefore, the effect on the oil pressure and oil film thickness is relatively small.

Due to pills at a certain speed shocking the tooth surface of spiral bevel gear continually, shot peening will cause the deformation of tooth surface and forming compressive stress in the subsurface of tooth. A suitable shot peening treatment will increase the lubrication characteristics of gear transmission. The microsurface lubrication characteristics formed

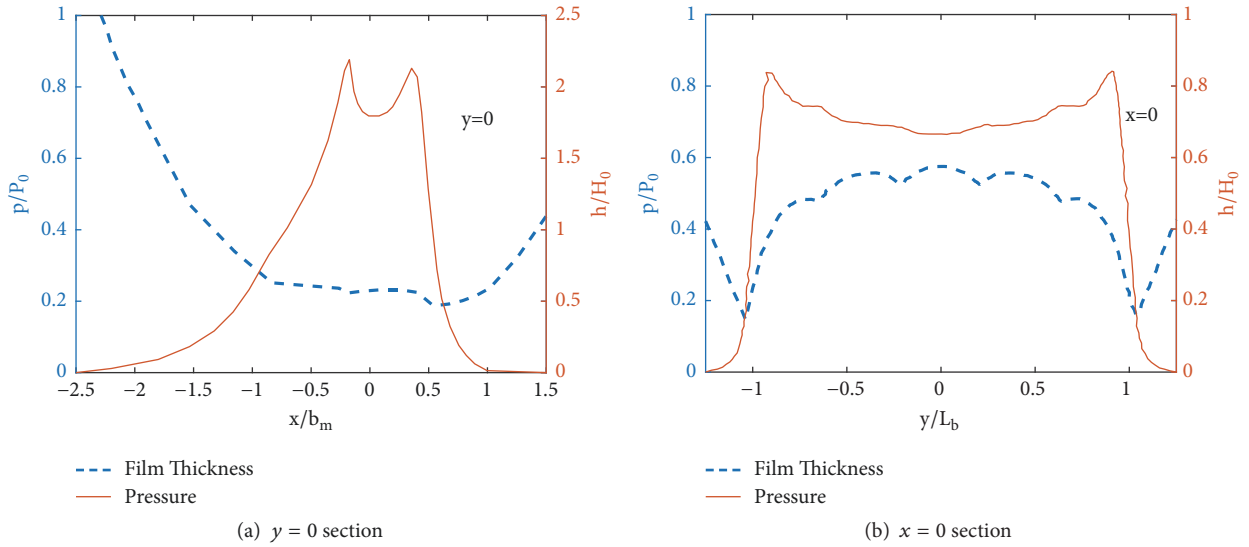


(a) $y = 0$ section (b) $x = 0$ section

Figure 9: Oil pressure and oil film thickness in meshing tooth surface of spiral bevel gear ($x = 0$ section).

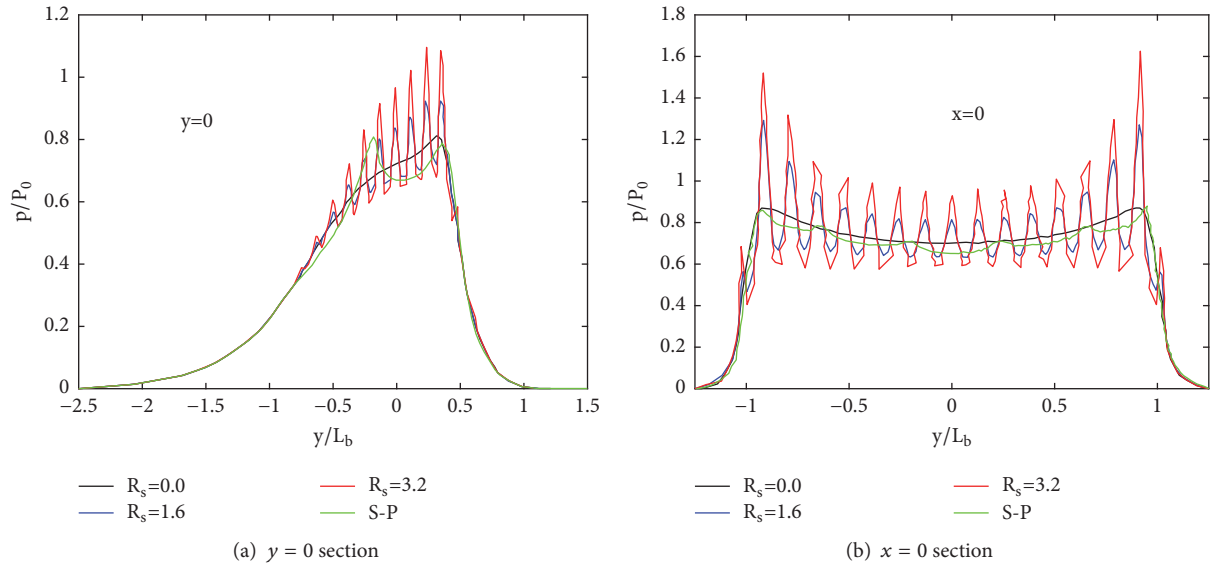


(a) $y = 0$ section (b) $x = 0$ section

Figure 10: Oil pressure distribution in meshing tooth surface of different surface roughnesses.

by shot peening are much better than those of the machined roughness model. For instance, for the cross section $y = 0$, compared with the $R_S = 3.2\,\mu$m, peak oil pressure value decreases from 1.15 $P_0$ to 0.8 $P_0$; the minimum oil film thickness increases from 0.4 $H_0$ to 0.5 $H_0$; peak oil pressure drops about 30%; and the minimum oil film thickness grows about 25%. For the cross section $x = 0$, oil pressure peak value drops from 1.6 $P_0$ to 0.8 $P_0$; in the center contact area the minimum oil film thickness increases from 0.45 $H_0$ to 0.55 $H_0$; the oil pressure peak value falls about 100%; and the minimum oil film thickness grows about 22%. As pits formed by shot peening, this kind of effect becomes even more remarkable.

From Figures 10 and 11, the effect of asperity on oil pressure and oil film thickness distribution reduces greatly as roughness gradually decreases. When the machining accuracy of the gear reaches the finishing machining, the lubrication characteristics of the gear are closer to the curve of $R_S = 0.0\,\mu$m. At this moment, the effect of shot peening on lubrication characteristics is either positive or negative, mainly depending on the final effect of shot peening on the surface roughness of the metal surface.

There is no doubt that the microstructure of tooth surface formed by shot peening decreases the effects of oil pressure and oil film thickness caused by asperity compared with the

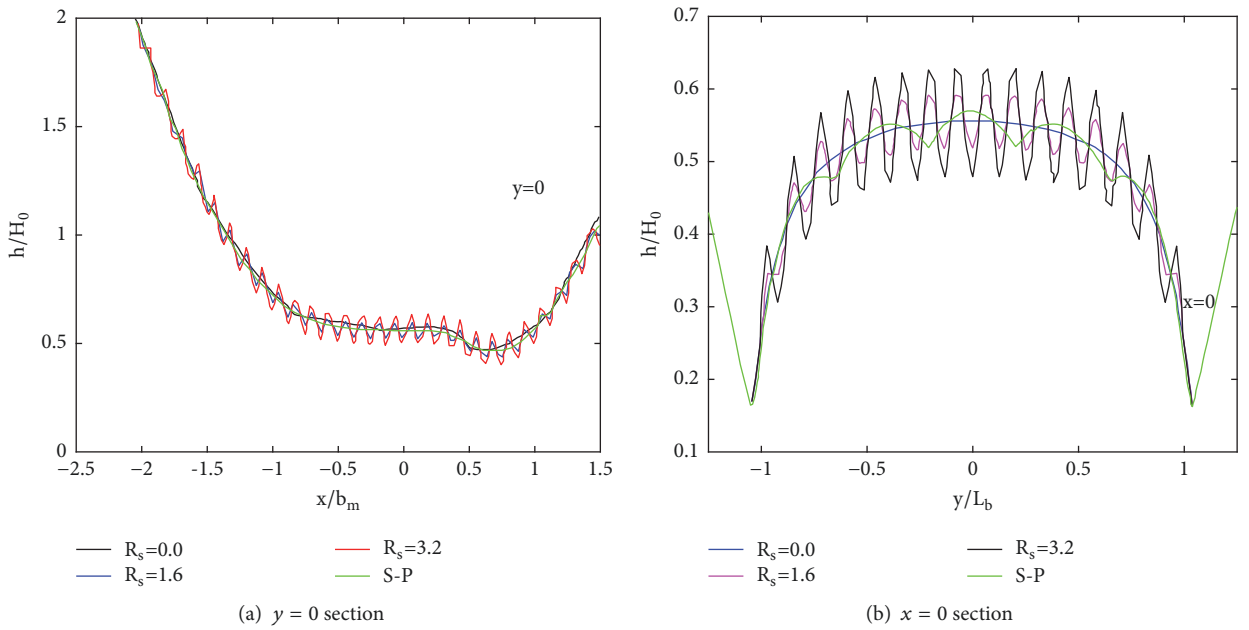


(a) $y = 0$ section (b) $x = 0$ section

Figure 11: Oil film thickness distribution in meshing tooth surface of different surface roughnesses.

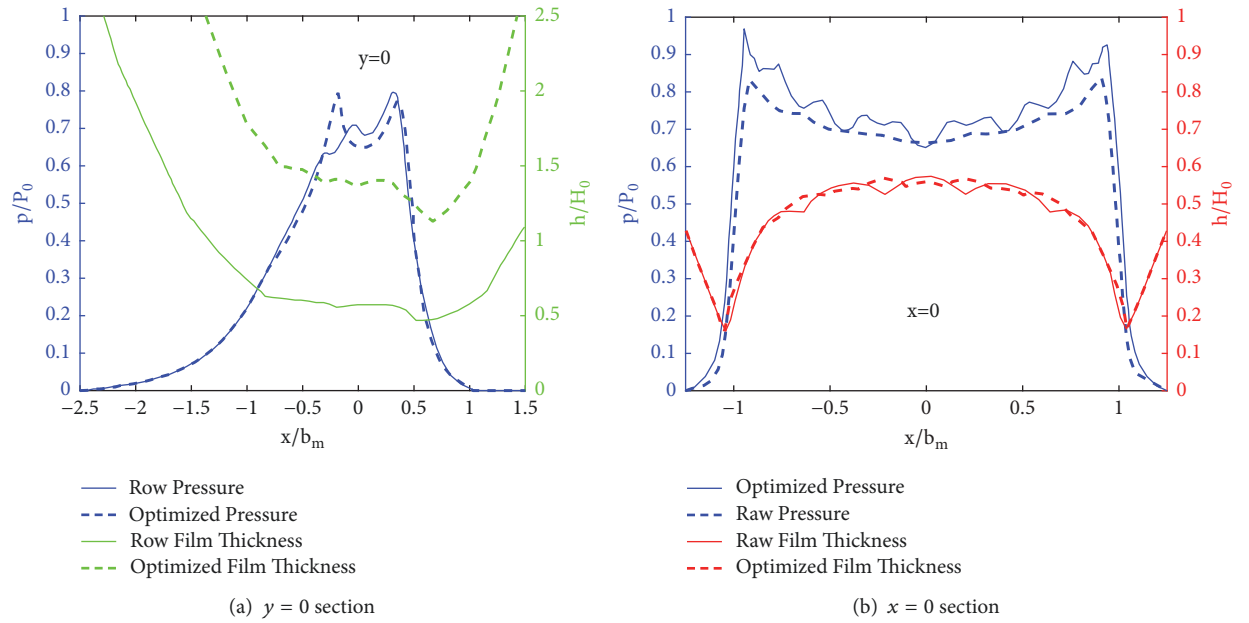


(a) $y = 0$ section (b) $x = 0$ section

Figure 12: The comparison between pressure distribution and thickness distribution.

machined tooth surface. The less the flow resistance is, the easier the oil film forms and, thus, it obtained a nice lubrication condition. In the same situation, the lubrication characteristics of shot peened spiral bevel gear are better than those of the machined gears.

Figure 12 is the contrastive images about oil pressure and oil film thickness distribution of original shot peening model and optimized shot-penning model on the cross section $y = 0$, $x = 0$. The 49-pellet model is the shot peening process before optimization, while the multiple-pellet model is the shot peening process after optimization. As shown in Figure 12, because of those pits and ridges, the asperity becomes finer and the fluctuation of oil pressure and oil film thickness is more apparent. With increasing intensity of shot peening, the overall roughness reduces on the gear surface, and the asperity effect weakens.

As shown in Figure 12(a), the first peak value on the cross section $y = 0$ falls from 0.8 $P_0$ to 0.63 $P_0$, and the pressure

drops about 21%. At the pressure collapse, on account of more serried asperity, the pressure of the collapse increases to some extent, from 0.65 $P_0$ to 0.7 $P_0$. Overall oil pressure is more evenly distributed. Meanwhile, as shown in Figure 12(b), the oil film thickness of cross section $y = 0$ has a remarkable increase, and the overall improvement is 0.5 $H_0$.

In the central contact area, the whole level of oil film thickness improves, gathering more lubrication oil there. From the cross section $x = 0$, the increase of asperities makes the fluctuation of pressure greater, but it is beneficial for the oil film thickness. The oil film thickness becomes more smooth and uniform, and the thickness of oil film increases as well, which is good for the improvement of lubrication performances.

## 5. Conclusion

Shot peening affects the roughness value and microstructure of tooth surface for spiral bevel gear. This paper established a reasonable FEA model that can describe the shot peened treatment of spiral bevel gear and obtained the coordinate of microstructure for tooth surface after shot peening, which reveals the elastohydrodynamic lubrication characteristics of spiral bevel gears after shot peening process by numerical method, especially for oil pressure and oil film thickness distribution in micro tooth surface during lubrication for different roughness conditions. This method can be used to predict the lubrication characteristics of spiral bevel gear at different surface roughness after shot peening treatment. The suitable shot parameters are favorable for lubrication, the oil film thickness can be increased, and the oil film thickness variation can be decreased. The oil pressure between the teeth can be increased and the oil pressure variation can be decreased. For the super smooth surface of spiral bevel gear, shot peening can not increase the lubrication of gear transmission.

After shot peening, the tooth surface topography of spiral bevel gear is reshaped and the dent has a stronger effect on the lubrication characteristics for meshing tooth surface of gear pair based on 49-pellet model. Pits are more likely to store lubricating oil, which is conducive to lubrication. At the same time, the bulge formed around the orange peel pits hinders the flowing of lubrication and thus increases gear wearing.

It can be predicted that if the shot peening coverage is further improved, the bulge formed around the orange peel pits will be weakened and then pits will become more finely divided. What is more, the main factors that affect lubrication will become the pit instead of the bulge around the pit. So, lubrication effect will be improved with the increase of coverage.

For rough or semi-finish process, the shot peened tooth surface is helpful. When the intensity of shot peening increases gradually, tool marks on the surface can be covered. However, adopting shot peening process to treat gears is not appropriate for finishing machining tooth surface, because shot peening will only make the gear surface rougher, and increasing roughness does no good for lubrication performance. Consequently, grinding process is necessary after shot peening.

## Nomenclature

$A$: Total area of contact area
$B$: Face wide
$b$: Half-width of Hertz contact
$C_w$: Coefficient of load
$E'$: Equivalent modulus of a pair of gear teeth material
$H_0$: Dimensionless film thickness of the rigid body center
$h_0$: Constant related to the film thickness of the rigid body center
$L_b$: Half-length of the contact line
$m$: Modulus of gear
$n$: Rotation rate
$P$: Pressure
$R$: Comprehensive curvature radius
$R_a$: Surface roughness
$R_s$: Amplitude of the cosine function asperity
$R_m$: Comprehensive curvature
$S$: Surface topography
$\overline{S}$: Dimensionless tooth surface morphology data
$T_p$: Torque
$t$: Time variable
$V$: Elastic deformation
$X$: Node coordinates
$x_{\text{in}}$: Initial point coordinate of the calculation region
$x_{\text{out}}$: End point coordinate of the calculation region
$Y$: Node coordinates
z: Teeth number
$z$: Viscosity index
$\alpha$: Viscosity coefficient
$\delta$: Pitch angle
$\eta$: Lubricating oil viscosity
$\eta_0$: Environmental viscosity
$\eta^*$: Equivalent viscosity of lubricating oil
$\mu_x$: Entrainment velocity of the tooth face
$\mu_m$: Entrainment velocity
$\tau$: Oil film shear stress
$\tau_0$: Reference shear stress
$\omega_n$: Target teeth carried load of each meshing moment
$\dot{\gamma}$: Shear rate
$\rho$: Density of the lubricating oil
$\rho_0$: Initial density
$\Delta\overline{h}$: Dimensionless thickness of the geometry gap
$\varepsilon_p$: Convergence criterion
$\varepsilon_w$: Convergence criterion.

## Data Availability

The data used to support the findings of this study are available from the corresponding author upon request.

## Conflicts of Interest

The authors declare that they have no conflicts of interest.

## Acknowledgments

This research is supported by Natural Science Foundation of Tianjin (no. 17JCQNJC04300), Open Funding of State Key Laboratory of Materials Processing and Die & Mould Technology-Huazhong University of Science and Technology (P2019-022), Open Funding of The State Key Laboratory of Mechanical Transmissions (no. SKLMT-KFKT-201616), Fundamental Research Funds for the Tianjin Universities (nos. 2017KJ083, TJPUZK20170118), National Natural Science Foundation of China (nos. 51475330, U1733108), National Training Program of Innovation and Entrepreneurship for Undergraduates (no. 201710058085), Applied Basic Research Project of China Textile Industry Association (no. J201806), and the Program for Innovative Research Team in University of Tianjin (no. TD13-5037). Thanks also are due to Professor Haruo Houjoh of Tokyo Institute of Technology, Professor Izhak Bucher of Israel Institute of Technology, Professor Yidu Zhang of Beihang University, Mr. Zhou Yao, and Ms. Wei Hong for their constant assistances.

## References

[1] L. Dimitrov, D. Michalopoulos, C. A. Apostolopoulos, and T. D. Neshkov, "Investigation of contact fatigue of high strength steel gears subjected to surface treatment," *Journal of Materials Engineering and Performance*, vol. 18, no. 7, pp. 939–946, 2009.

[2] L. Guo, S. Zhou, L. Crocker, and A. Turnbull, "Initiation sites for cracks developed from pits in a shot-peened 12Cr martensitic stainless steel," *International Journal of Fatigue*, vol. 98, pp. 195–202, 2017.

[3] S. Li and A. Anisetti, "A tribo-dynamic contact fatigue model for spur gear pairs," *International Journal of Fatigue*, vol. 98, pp. 81–91, 2017.

[4] C. Zhou, Z. Xiao, S. Chen, and X. Han, "Normal and tangential oil film stiffness of modified spur gear with non-Newtonian elastohydrodynamic lubrication," *Tribology International*, vol. 109, pp. 319–327, 2017.

[5] D. Gallitelli, V. Boyer, M. Gelineau et al., "Simulation of shot peening: from process parameters to residual stress fields in a structure," *Comptes Rendus (Doklady) de l'Academie des Sciences de l'URSS*, vol. 344, no. 4-5, pp. 355–374, 2016.

[6] Y. Lv, L. Lei, and L. Sun, "Effect of microshot peened treatment on the fatigue behavior of laser-melted W6Mo5Cr4V2 steel gear," *International Journal of Fatigue*, vol. 98, pp. 121–130, 2017.

[7] A. Terrin, C. Dengo, and G. Meneghetti, "Experimental analysis of contact fatigue damage in case hardened gears for off-highway axles," *Engineering Failure Analysis*, vol. 76, pp. 10–26, 2017.

[8] W. Pu, J. Wang, R. Yang, and D. Zhu, "Mixed elastohydrodynamic lubrication with three-dimensional machined roughness in spiral bevel and hypoid gears," *Journal of Tribology*, vol. 137, no. 4, Article ID 041503, pp. 1–11, 2015.

[9] C.-B. Tang, D.-X. Liu, B. Tang, X.-H. Zhang, L. Qin, and C.-S. Liu, "Influence of plasma molybdenizing and shot-peening on fretting damage behavior of titanium alloy," *Applied Surface Science*, vol. 390, pp. 946–958, 2016.

[10] B. AlMangour and J.-M. Yang, "Improving the surface quality and mechanical properties by shot-peening of 17-4 stainless steel fabricated by additive manufacturing," *Materials and Corrosion*, vol. 110, pp. 914–924, 2016.

[11] D. Trauth, J. Stanke, A. Shirobokov, P. Mattfeld, and F. Klocke, "Analysis of the fluid pressure, load capacity, and coefficient of friction of an elliptic machine hammer peened surface structure in hydrodynamic lubrication," *Production Engineering Research and Development*, vol. 10, no. 6, pp. 539–550, 2016.

[12] V. V. Simon, "Optimal tooth modifications in face-hobbed spiral bevel gears to reduce the influence of misalignments on elasto-hydrodynamic lubrication," *Journal of Mechanical Design*, vol. 136, no. 7, Article ID 071007, pp. 1–9, 2014.

[13] M. Shuai, Z. Yidu, and W. Qiong, "Research on multiple-split load sharing of two-stage star gearing system in consideration of displacement compatibility," *Mechanism and Machine Theory*, vol. 88, pp. 1–15, 2015.

[14] M. Shuai and Z. Yidu, "Spiral bevel gear true tooth surface precise modeling and experiments studies based on machining adjustment parameters," *Proceedings of the Institution of Mechanical Engineers, Part C: Journal of Mechanical Engineering Science*, vol. 229, no. 14, pp. 2524–2533, 2015.

[15] S. H. Yuan, H. L. Dong, and X. Y. Li, "Analysis of lubricating performance for involute gear based on dynamic loading theory," *Journal of Mechanical Design*, vol. 134, no. 12, Article ID 121004, pp. 67–75, 2012.